Protein Folding in Membranes: Insights from Neutron Diffraction Studies of a Membrane β-Sheet Oligomer

Xue Han,* Kalina Hristova,* and William C. Wimley†
*The Johns Hopkins University, Department of Materials Science and Engineering, Baltimore, Maryland 21218; and †Tulane University Health Sciences Center, Department of Biochemistry, New Orleans, Louisiana 70112

ABSTRACT Studies of the assembly of the hexapeptide Acetyl-Trp-Leu$_5$ (AcWL$_5$) into β-sheets in membranes have provided insights into membrane protein folding. Yet, the exact structure of the oligomer in the lipid bilayer is unknown. Here we use neutron diffraction to study the disposition of the peptides in bilayers. We find that pairs of adjacent deuterium-labeled leucines have no well-defined peak or dip in the transmembrane distribution profiles, indicative of heterogeneity in the depth of membrane insertion. At the same time, the monomeric homolog AcWL$_4$ exhibits a homogeneous, well-defined, interfacial location in neutron diffraction experiments. Thus, although the bilayer location of monomeric AcWL$_4$ is determined by hydrophobicity matching or complementarity within the bilayer, the AcWL$_5$ molecules in the oligomer are positioned at different depths within the bilayer because they assemble into a staggered transmembrane β-sheet. The AcWL$_5$ assembly is dominated by protein-protein interactions rather than hydrophobic complementarity. These results have implications for the structure and folding of proteins in their native membrane environment and highlight the importance of the interplay between hydrophobic complementarity and protein-protein interactions in determining the structure of membrane proteins.

INTRODUCTION

The folding of hydrophobic polypeptide segments of membrane proteins in their native environment occurs in the context of the highly anisotropic lipid bilayer. About half of the thickness of the lipid bilayer is attributed to the essentially nonpolar hydrocarbon core, whereas the other half is the chemically heterogeneous bilayer-water ''interface'' (1,2). The bilayer is thus characterized by a complex distribution of hydrophobicity (or polarity) along the bilayer normal (3). A prevailing view of protein folding in membranes is that the complementarity between the hydrophobicity of an embedded segment and the bilayer hydrophobicity profile is the predominant driving force determining polypeptide disposition across the bilayer (3,4). Specific protein-protein interactions occur within the structural bounds determined by this complementarity. An alternative scenario can be considered in which protein-protein interactions can be a predominant driving force for membrane protein folding, such that the hydrophobic complementarity can be compromised to satisfy protein-protein interactions (5–8). In this article, we address this issue by determining the depth of penetration of amino acids within the membrane-embedded oligomer of the hexapeptide Acetyl-Trp-Leu$_5$ (AcWL$_5$) and its monomeric homolog Acetyl-Trp-Leu$_4$ (AcWL$_4$).

The hexapeptide AcWL$_5$ has been used as a model system for studying folding of proteins in membranes (9–12). Based on numerous biophysical experiments, a hypothetical model was proposed in which AcWL$_5$ forms antiparallel β-sheets that are centered in the hydrocarbon core in the bilayer. Although we know that hydrogen bonding is the main driving force for folding of AcWL$_5$ in membranes (11), this model also contains the implicit assumption that hydrophobic complementarity determines the transbilayer disposition of the peptide. In the work presented here, we used neutron diffraction to study the transbilayer distribution of AcWL$_5$, and we found no well-defined position of selected leucines within the bilayer thickness. Thus, the peptide must be forming an asymmetric or staggered β-sheet across the bilayer, and hydrophobic complementarity is not the only determinant of the oligomer structure. Instead, the structure of the assembled AcWL$_5$ oligomer is largely determined by protein-protein interactions, particularly backbone hydrogen bonding within the membrane.

Although these results are obtained for a membrane-embedded peptide β-sheet, we propose that they can be generalized to highlight a principle of membrane protein folding that applies to transmembrane (TM) helices also.

MATERIALS AND METHODS

Peptide synthesis

Fmoc amino acids, Leu, Trp, and Trp(Boc), were purchased from Novabiochem (San Diego, CA), and deuterated Fmoc amino acid, Fmoc-Leu (D10, side chain completely deuterated), was from CDN isotope (Pointe-Claire, Quebec). Preloaded Fmoc-Leu Wang resin (~0.9 mmol/g) and 2-chlorotrityl resin (~1 mmol/g) were obtained from Advanced Chemtech (Louisville, KY).

The peptides Acetyl-Trp-Leu-Leu-Leu-Leu (AcWL$_4^H$) and Acetyl-Trp-Leu(D10)-Leu(D10)-Leu-Leu(AcWL$_4^D$) were synthesized via solid-phase peptide synthesis on a model 431 ABI peptide synthesizer using Fmoc chemistry (13–15). The peptides Acetyl-Trp-Leu-Leu-Leu-Leu-Leu (AcWL$_5^H$), Acetyl-Trp-Leu(D10)-Leu(D10)-Leu-Leu-Leu (AcWL$_5^{D23}$), and

Submitted May 18, 2007, and accepted for publication August 28, 2007.

Address reprint requests to Kalina Hristova, The Johns Hopkins University, Dept. of Materials Science and Engineering, Baltimore, MD, 21218. Tel.: 410-516-8939; Fax: 410-516-5239; E-mail: kh@jhu.edu.

Editor: Thomas J. McIntosh.

0006-3495/08/01/492/14 $2.00

doi: 10.1529/biophysj.107.113183

Acetyl-Trp-Leu-Leu-Leu-Leu(D10)-Leu(D10) ($AcWL_5^{D56}$), were synthesized as described previously (12). The identity of each peptide was confirmed by MALDI-TOF mass spectrometry, and purification was done using a VyDAC 218TP510 C18 column using a water/acetonitrile gradient in the presence of 0.1% trifluoroacetic acid. Circular dichroism (CD) and fluorescence spectroscopy in membranes, described below, were used to demonstrate identical structure, folding, and membrane interaction for each peptide synthesized.

Neutron sample preparation and data analysis

1-Palmitoyl-2-oleoyl-*sn*-glycero-3-phosphocholine (POPC) was purchased from Avanti Polar Lipids (Alabaster, AL), and D_2O was from Cambridge Isotope Labs (Andover, MA). Purified peptides were dissolved in methanol, and their concentrations were determined using the tryptophan absorbance at 284 nm. Mutilayer samples containing 5 mol % $AcWL_4^H$, $AcWL_4^D$, $AcWL_5^H$, $AcWL_5^{D23}$, or $AcWL_5^{D56}$ were prepared by mixing POPC in chloroform and peptides in methanol in appropriate ratios and depositing on a thin glass slide, followed by complete evaporation of the solvents in vacuum. The multilayer sample size was ~12 mm × 12 mm × 0.5 μm.

Neutron diffraction experiments were performed at the Advanced Neutron Diffractometer/Reflectometer at the National Institute of Standards and Technology center for Neutron Research, Gaithersburg, MD. Relative humidity (RH) of 76% was achieved using a saturated NaCl solution, as described (16). Each multilayer sample was hydrated using H_2O mixed with 0%, 20%, and 40% D_2O. The wavelength of the neutron beam was 4.99 Å.

Neutron diffraction experiments and data analysis have already been described in detail (16). Structure factors were calculated as the square root of the integrated intensities after absorption and Lorentz factor corrections, and phases were assigned as previously described (16). We adopted the so-called ''absolute'' scale, ''scattering length per lipid per unit length (i.e., per unit bilayer thickness)'', defined by White and colleagues (17–20). Diffraction intensities were measured at 3 different H_2O/D_2O ratios for each sample at 76% RH. As discussed previously, data collection for various H_2O/D_2O ratios allows the determination of the phases of the structure factors (16). It also allows us to reduce the random noise in the experimental data (20,21), which is important because large random errors in the experimental structure factors can obscure the contrast provided by the deuterium label. The random errors in the experimental structure factors are minimized by placing the structure factors for each peptide on a self-consistent arbitrary scale and linearizing them with D_2O concentration, as described previously (16). The fact that such linearization was achieved (see Fig. 4) demonstrates that the D_2O/H_2O replacement is isomorphous, as expected (16,20).

Data collected for different bilayers can be compared only if the structure factors and the profiles are scaled and placed on an absolute (per lipid) scale (17). Determination of the absolute profiles requires knowledge of the unit cell contents as well as the instrumental constants k, which are the scale factors that relate the experimentally determined structure factors to the absolute structure factors (22). As discussed previously (20,21), the instrumental constants and the absolute structure factors can be determined by comparing the scattering profiles of two samples with isomorphous unit cells that have the same structure except for a few atoms with different scattering lengths. The difference in scattering acts as a ''label'' for the substituted atoms.

The relation between the absolute profiles $\rho(z)$ and the scaled absolute structure factors $F(h)$ is given by:

$$\rho^*(z) = \rho(z)S = \rho_0^* + \frac{2}{d} \times \frac{1}{k} \sum_{h=1}^{h_{obs}} f(h) \cos\left(\frac{2\pi h z}{d}\right),$$

where d is the Bragg spacing, ρ_0^* is the average scattering length density of the unit cell calculated from the known sample compositions, and h_{obs} is the highest observed diffraction order. This equation was used to produce the profiles shown below (see Figs. 5 *A*, 6, 7 *A*, and 8 *A*).

Methods for structure factors scaling: an overview

Two methods were used to scale the structure factors: the ''real space'' and the ''reciprocal space'' scaling methods.

The "real space" scaling method

This method was used by Wiener and White to scale fully resolved 1,2 dioleoyl-*sn*-glycero-3 phosphocholine profiles at low hydrations (20). The idea behind the scaling is that the profiles of the isomorphous unit cells are identical in a region that is never visited by the labeled moiety. Two points, z_1 and z_2, within this region are used in equations describing the profile overlap to determine the instrumental constants for the two isomorphous samples. Then, the parameters of the label distributions are found by fitting Gaussian distributions to the difference profiles.

For profiles that are not fully resolved, the calculated absolute structure factors may depend on the choice of z_1 and z_2 (21). In addition, the fitting is based on the a priori assumption that the two profiles overlap completely at z_1 and z_2.

The "reciprocal space" scaling method

A modified procedure was used by Hristova and White (21) that allows precise scaling of both fully resolved and underresolved profiles, provided that at least four structure factors are observed. This procedure takes into account that the experimentally observed label distributions are Gaussian and gives the instrumental constants and the parameters of the Gaussian distribution in one step by minimizing the difference between calculated and experimentally observed structure factors.

Isomorphous labeling

In the neutron diffraction experiments, contrast was introduced in two ways: 1), by incorporating peptides with deuterated amino acids and 2), by exchanging a fraction of the hydrating water with heavy water. Thus, the ''label'' used in the scaling procedure could be either the 1), deuterons of the leucine side chains or 2), the deuterons of the hydrating water molecules. Both labels can be used to scale the data, provided that the number of deuterons per unit cell is known. The peptide/lipid ratio was chosen as desired during sample preparation (after careful measurements of peptide and lipid concentrations), and therefore, the number of protein-associated deuterons is known. In the experimental setup, however, the number of water molecules could not be chosen as desired. Although the RH of the atmosphere is controlled, the amount of water taken up by the bilayer depends on the bilayer structure and the incorporated peptides. Generally, bilayers with peptides take up water differently than pure bilayers (23,24). Because of the uncertainty in the number of waters per unit cell, previously scaling has been performed using labels associated with lipids or peptides (20,21,23,24).

Water uptake was measured gravimetrically, as described below. These measurements are, however, associated with an experimental uncertainty because of waters that remain associated with the bilayer even under vacuum (see below). This uncertainty affected the calculated instrumental constants and the absolute scattering profiles. However (see Figs. 7 *C* and 8 *C*), the difference profiles describing the distribution of deuterated leucines were not affected.

Calculations of water distributions

The water distribution across the bilayers was determined by fitting Gaussians to the difference between the profiles acquired for 0% D_2O and 20% D_2O using the ''reciprocal space'' scaling method. For $AcWL_4$, the fit gave the position and width of the water distribution and the number of water

molecules per lipid. For $AcWL_5$, the profiles were scaled assuming hydration of five water molecules per lipid. This fit gave the position and width of the water distribution and the instrumental constants in one step.

Spectroscopy

Fluorescence spectroscopy was performed on a Fluorolog-3 fluorometer (Jobin Yvon, Edison, NJ). An excitation wavelength of 290 nm was used, and excitation and emission slits were 2 nm. POPC multilayers with 5 mol % $AcWL_4$ or $AcWL_5$ were prepared in the same manner as neutron diffraction samples. The multilayers were deposited on a $25 \times 25 \times 5$ mm quartz glass slide, which was placed in the sample chamber. Measurements were performed at 76% and 100% RH, which were achieved using a saturated solution of NaCl and distilled water, respectively. The angle between the slide and the incident beam was 35° (25).

CD measurements were performed using a 1 mm cuvette with a Jasco J710 spectrometer. Phosphate buffer (10 mM, pH = 7) was used because of its weak near-UV absorbance. Samples of 5 mol % $AcWL_4^H$, $AcWL_4^D$, $AcWL_5^H$, $AcWL_5^{D23}$, and $AcWL_5^{D56}$ in POPC unilamellar vesicles were prepared by the following method: the peptide was first dissolved in methanol; the methanol was removed, extruded unilamellar POPC vesicles in phosphate buffer were added to the dry peptides, and the sample was equilibrated by cycling three times between room temperature and 90°C.

Oriented circular dichroism (OCD) measurements were performed with multilayer samples of POPC containing 5 mol % $AcWL_4^H$, $AcWL_4^D$, $AcWL_5^H$, $AcWL_5^{D23}$, and $AcWL_5^{D56}$, at 76% and 100% RH. Experimental details are described elsewhere (23,26).

Determination of sample hydration

The weight of a glass slide was measured in vacuum and in a 76% RH environment, and the difference was negligible. Multilayer samples of lipids and peptides were prepared in the same way as for neutron diffraction experiments. After deposition, the samples were placed in vacuum overnight. The weights were measured as dry weights. Then the samples were hydrated in a humidity chamber for 6 h to overnight. The weights of the samples were then measured as the wet weights. The difference between the wet weight and the dry weight was the weight of the water taken up. This procedure was repeated 10 times, and the average was used to calculate the number of water molecules per lipid. The humidity chamber was a desiccator with NaCl solution inside instead of desiccants.

Measurements with pure bilayers have shown that there are a minimum of 0.2 residual waters per lipid associated with thoroughly dried lipids (27). Our own control measurements with pure bilayers showed that one water molecule remained associated with each lipid under ''dry'' conditions. We assumed that the same is true for bilayers with peptides, such that the measured hydration was corrected by adding a water molecule per lipid. It is possible that additional water molecules may remain associated with the peptides under vacuum. Thus, gravimetric measurements of water content may have uncertainties in addition to the experimental errors (i.e., standard deviations derived from 10 separate measurements) reported below. These uncertainties impact the scaling of the structure factors and the amplitudes of the scattering profiles but not the final results for the transbilayer distribution of the leucine labels (see Figs. 7 *C* and 8 *C*), which are derived from difference profiles.

Molecular modeling

Molecular modeling was used to compare the observed depth distributions of deuterons from neutron diffraction to the distributions obtained from putative structures of $AcWL_5$ and $AcWL_4$. We used a database of leucine residues in random configurations from the protein data bank (28) to determine the hard-sphere distribution of side-chain protons in leucine residues. The distribution was Gaussian and had a $1/e$ half-width of 3.06 Å. We then convoluted the ''hard sphere'' distribution of deuterons across the bilayer with a conservatively large *B*-factor of 200 Å to give an effective Gaussian $1/e$ half-width of 4.66 Å. The *B*-factor is derived from diffraction studies (1,23) and takes into account the thermal disorder in the bilayer, with the assumption that the peptide thermal disorder is similar to the largest lipid thermal disorder. We started with a molecular model of an ideal octameric, antiparallel β-sheet of $AcWL_5$ (12) in which the β-sheets and β-strands are perpendicular to the bilayer. In the model the β-sheets have no twist. We then determined the possible distributions of deuterons of the two pairs of adjacent leucines (L2-L3 and L5-L6) for various hypothetical transbilayer structures in which we maintained the parallel orientation of the strands but staggered them, thus changing the distributions of strands within the sheet. All hypothetical models that were roughly symmetric (see, e.g., Fig. 11 *A*) produced peaks in the deuteron distributions that were larger than the experimentally observed distributions. Only models with a nonsymmetric stagger between β-strands (see Fig. 11, *B* and *C*) were consistent with the experimental data, giving no high-contrast peaks in the transbilayer profile.

RESULTS

We have previously shown that neutron diffraction can be used to determine the location of groups of amino acids in a TM α-helix in bilayers with respect to the bilayer normal (16). In this work, we extend the methodology to the unstructured peptide $AcWL_4$ and to the peptide $AcWL_5$, known to form β-sheets in bilayers. The main goal of this work was to determine the structure of $AcWL_5$ in the bilayer by determining the depth of penetration of its deuterated leucines. These results were compared with results for $AcWL_4$, known to reside in the interfacial region as a monomer (29).

We synthesized five peptides, $AcWL_4^H$, $AcWL_4^D$, $AcWL_5^H$, $AcWL_5^{D23}$, and $AcWL_5^{D56}$. In each deuterated peptide, two leucines were deuterated, introducing 20 deuterons per peptide (Fig. 1 *A*). We have previously shown that at least 10 deuterons per peptide, at peptide concentration of a few mole percent, are required for sufficient contrast in the neutron diffraction experiments (16).

Neutron diffraction results for $AcWL_4$

$AcWL_4$ is an unstructured peptide used for the development of the first experimentally based membrane hydrophobicity scale (29). Here we used neutron diffraction to determine the transbilayer distribution of two of its leucines (see Fig. 1 *A*) within the bilayer. Such neutron diffraction experiments rely on the assumption that replacing amino acids with deuterated ones does not affect the structure of the peptides or of the bilayer with incorporated peptides. Fig. 1 *B* shows the CD spectra of $AcWL_4^H$ (*solid line*) and $AcWL_4^D$ (*dashed line*) in a phosphate buffer in the presence of POPC large unilamellar vesicles. The CD spectra, with minima at ~200 nm, are characteristic of random coil peptides (30) and are identical, as expected. The OCD signals of the two peptides are also identical (Fig. 2 *A*) because the observed differences in amplitudes are not statistically significant.

Neutron diffraction experiments were carried out with POPC multilayers with 5 mol % $AcWL_4^H$ and $AcWL_4^D$. The

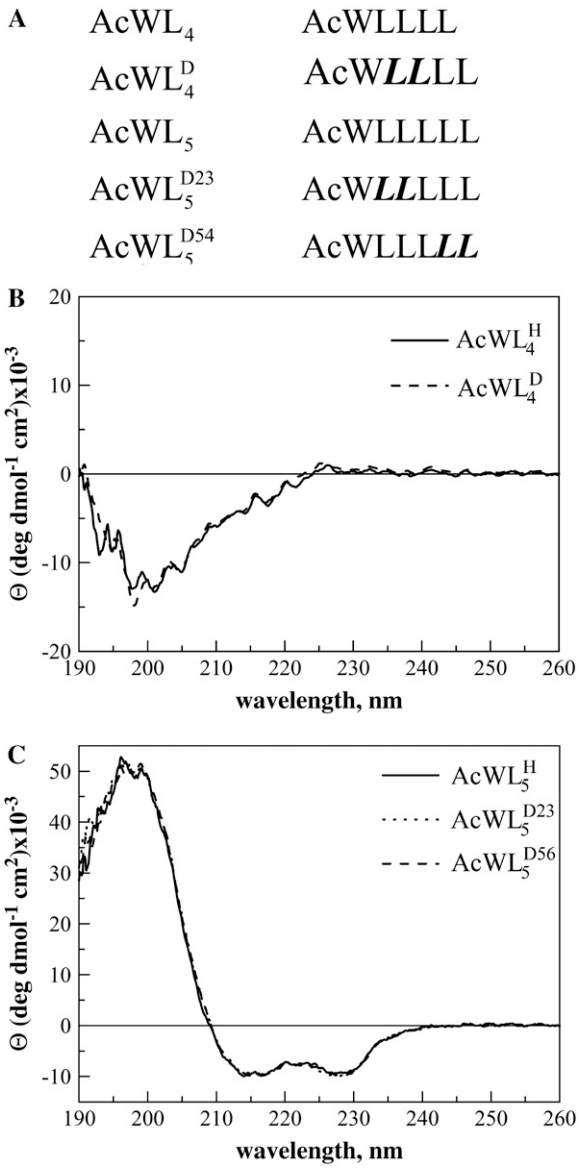

FIGURE 1 (*A*) Amino acid sequences of the five peptides studied here. $AcWL_4$ partitions into bilayer interfaces as a monomer, whereas $AcWL_5$ forms β-sheet oligomers. The deuterated amino acids are shown in bold. (*B*) CD spectra of $AcWL_4$ (*solid line*) and $AcWL_4^D$ (*dashed line*) in phosphate buffer (pH = 7) in the presence of POPC unilamellar vesicles. The spectrum is characteristic of unstructured proteins. (*C*) CD spectra of $AcWL_5^H$ (*solid line*), $AcWL_5^{D23}$(*dotted line*), and $AcWL_5^{D56}$ (*dashed line*) in a phosphate buffer (pH = 7) in the presence of POPC large unilamellar vesicles. The spectra, with minima at 215 nm and strong maxima at 198 nm, are characteristic of an antiparallel β-sheet structure. The peak in the vicinity of 230 nm is caused by tryptophan (32). All the spectra were measured in a 1mm cuvette containing 68 μM peptide in 10 mM phosphate solution of 1.3 mM POPC vesicles.

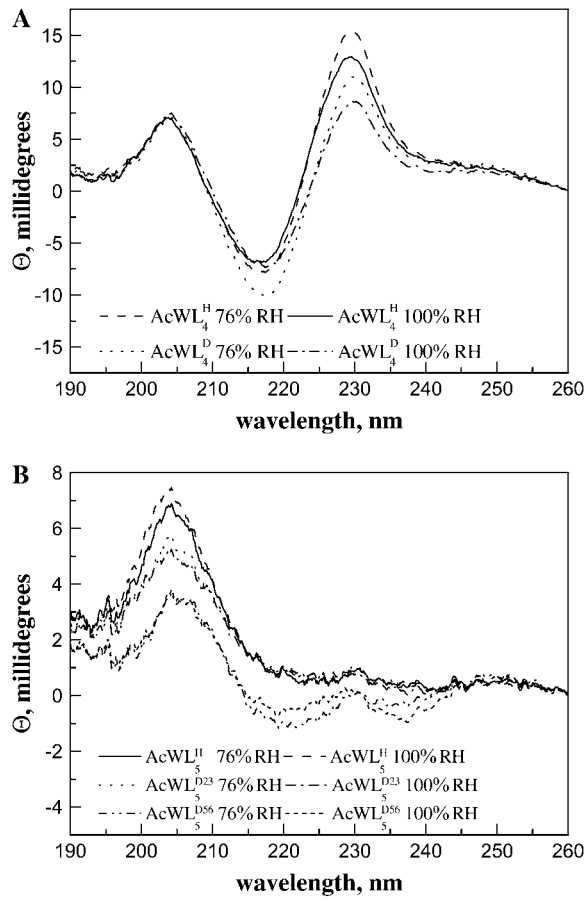

FIGURE 2 (*A*) Oriented CD spectra of 5 mol % $AcWL_4$ and $AcWL_4^D$ in POPC multilayers, equilibrated at 76% and 100% RH. (*B*) Oriented CD spectra of 5 mol % $AcWL_5$, $AcWL_5^{D23}$ and $AcWL_5^{D56}$ in POPC multilayers, equilibrated at 76% and 100% RH. Peptides and lipids (molar ratio 1:19) were mixed in methanol/chloroform, deposited on a quartz slide, and hydrated to form multilayers. Note that the amplitude of the signal depends on the thickness of the sample, which is hard to control. Thus, the observed difference in amplitude in the experimental spectra is not statistically significant (15,16).

diffraction patterns were indicative of lamellar phases with Bragg spacing of ~51 Å. Importantly, the width of all four observed diffraction peaks was identical, indicative of lack of lattice disorder and fully resolved, thermally disordered structures (18) (see Fig. 3 for a typical diffraction pattern). The mosaic spread was low; a typical full-width at half-maximum was 0.6°. The Bragg spacings for $AcWL_4^H$ or $AcWL_4^D$ were very similar, an indication that the underlying structure of the bilayer with incorporated peptide does not change in the presence of the deuterium label.

Structure factors were first scaled using the reciprocal space scaling method, as described in Materials and Methods. The isomorphous substitution utilized in the scaling was the exchange of 20 hydrogens with deuterons within the protein leucines. The structure factors were measured for three different H_2O/D_2O ratios, and the random errors in the experimental structure factors were minimized by placing the structure factors for each peptide on a self-consistent arbitrary scale and linearizing them with D_2O concentration before scaling. The absolute structure factors are plotted in Fig. 4 as a function of D_2O content, the values at 0% D_2O are

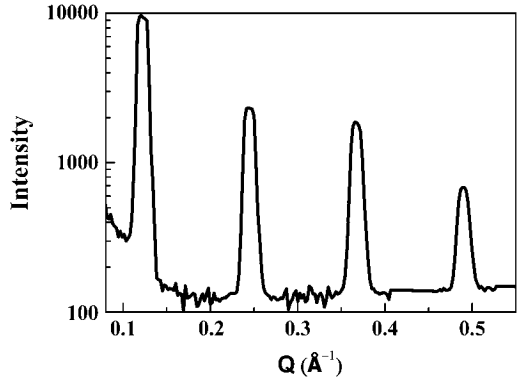

FIGURE 3 Raw neutron diffraction data recorded for POPC bilayers with 5 mol % $AcWL_5$, 100% H_2O, 76% RH.

shown in Table 1, and the difference structure factors are shown in Table 2. The absolute scattering length density profiles of POPC bilayers containing 5% $AcWL_4^H$ (*solid line*) and $AcWL_4^D$ (*dashed line*) are shown in Fig. 5 *A*. The absolute difference profile (Fig. 5 *B*), a result of the direct subtraction of the two absolute profiles, corresponds to the transbilayer distribution of the deuterium label in $AcWL_4^D$. The absolute difference profile has a maximum at ~17 Å from the bilayer center and reaches zero scattering length at the midplane of the bilayer, consistent with the expectation that $AcWL_4$ does not penetrate deep into the bilayer hydrocarbon core (29). The distribution of the label is well described by two Gaussians, centered at 17.2 ± 0.1 Å with a 1/*e* half-width of 7.1 ± 0.1 Å. These errors are calculated as described (1,21). Thus, the neutron diffraction results provide a direct proof that $AcWL_4$ is located in the interfacial region of the bilayer.

Because the deuterium label is assumed not to reside in the center of the bilayer, the data were also scaled using the real space-scaling method. For any choice of z_1 and z_2 close to the bilayer center, this alternative fitting procedure yielded a Gaussian distribution with center 17.2 ± 0.1 Å and 1/*e* half-width 7.1 ± 0.1 Å, identical to the results for the reciprocal space-scaling method. Thus, the calculated distribution of the label is not affected by the choice of z_1 and z_2 or the method of scaling. This is an indication that the profile is fully resolved; i.e., no structure factors are lost as a result of peak widening until the peak is lost in the noise because of lattice disorder (31).

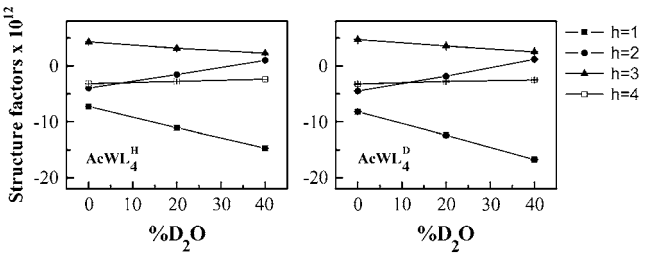

FIGURE 4 Absolute structure factors of POPC bilayers with 5 mol % $AcWL_4$ and $AcWL_4^D$ as a function of D_2O mole percentage. The structure factors were scaled as described in Materials and Methods, using the reciprocal space-scaling method. The experimental uncertainties were calculated as described previously (16). The linear dependence of the structure factors on D_2O mole percentage shows that the H_2O/D_2O exchange is an isomorphous replacement. These plots were used to determine the signs of the structure factors (Table 1), as described (20,21).

The water uptake of the bilayer was determined by comparing absolute profiles of bilayers hydrated in 100% H_2O, i.e., 0% D_2O (shown in Fig. 5 *A*), and 80% H_2O + 20% D_2O (not shown). By fitting Gaussians to the absolute difference profiles, we determined the center and the width of the water distribution in the presence of $AcWL_4$ as 24.6 Å and 6.1 Å, respectively, as well as the number of water molecules per lipid as 5.6 waters per molecule (see Fig. 9 *A*). The fitted water Gaussians are shown in dashed lines. The solid lines, which closely follow the experimental profiles (*thick dotted lines*), are the envelopes of the two water Gaussians from apposing bilayers.

To verify the calculations of water uptake by the bilayer in the presence of $AcWL_4$, we measured the number of water molecules gravimetrically, as described in Materials and Methods. The measured value was 5 ± 1 waters per lipid. Thus, the calculation produced a value that was within the experimentally determined range.

Neutron diffraction results for $AcWL_5$

$AcWL_5$ behaves very differently in bilayers, as compared with $AcWL_4$. Whereas $AcWL_4$ is an interfacially bound random coil, $AcWL_5$ cooperatively self-assembles in membranes into highly ordered, oligomeric β-sheets (9–12). Fig. 1 *B* shows the CD spectra of $AcWL_5^H$ (*solid line*), $AcWL_5^{D23}$ (*dashed line*), and $AcWL_5^{D56}$ (*dotted line*) in phosphate buffer with POPC large unilamellar vesicles. The spectra of membrane-bound $AcWL_5$, characterized by minima at 215 nm and strong maxima at 198 nm, are highly characteristic of classical antiparallel β-sheet structures (12). The peak in the vicinity of 230 nm is caused by tryptophan (32). The overlap among the three spectra indicates that the three peptides behave in the same way under the experimental conditions. The H/D exchange does not change their biophysical properties in terms of membrane partitioning and folding. The OCD spectra of the three peptides are also very similar (Fig. 2 *B*).

Neutron diffraction experiments were carried out with POPC multilayers with 5 mol % $AcWL_5^H$, $AcWL_5^{D23}$, and $AcWL_5^{D56}$. The measured Bragg spacing was 51.3 Å for all three multilayer samples, consistent with the fact that the underlying structure of the bilayer with incorporated peptide does not change in the presence of the deuterium label.

An attempt was made to scale the structure factors using the reciprocal space scaling method, similarly to the fit carried out for $AcWL_4$, by comparing structure factors between

TABLE 1 Observed absolute structure factors and their experimental uncertainties for POPC multilayers with 5 mol % peptide at 76% RH

h*	POPC	$AcWL_4^H$	$AcWL_4^D$	$AcWL_5^H$	$AcWL_5^{D23}$	$AcWL_5^{D56}$
1	−7.95	−7.28 ± 0.03	−8.21 ± 0.03	−4.99 ± 0.01	−4.89 ± 0.02	−4.83 ± 0.02
2	−4.27	−3.97 ± 0.02	−4.48 ± 0.04	−3.39 ± 0.01	−3.19 ± 0.01	−3.13 ± 0.01
3	4.85	4.31 ± 0.03	4.72 ± 0.03	3.65 ± 0.01	3.55 ± 0.02	3.36 ± 0.01
4	−3.48	−3.17 ± 0.04	−3.24 ± 0.02	−2.37 ± 0.01	−2.55 ± 0.02	−2.19 ± 0.02
5	−0.56			−0.50 ± 0.03	−0.36 ± 0.04	−0.48 ± 0.04
k†		0.49 ± 0.04	0.56 ± 0.04	0.45 ± 0.03	0.41 ± 0.03	0.46 ± 0.03
R_{self}‡		0.035	0.030	0.0034	0.0046	0.0049
R_{difff}§			0.10		0.050	0.044
d (Å)¶	52.4 ± 0.2	51.7 ± 0.3	51.1 ± 0.3	51.3 ± 0.3	51.3 ± 0.3	51.3 ± 0.3

*Diffraction order.
†Instrumental constants (i.e., scaling factors), which are determined by experimental details such as the amount of sample of the beam, etc.
‡Self R factor, $R_{self} = \sum_{h=1}^{h_{obs}} |\sigma(h)| / \sum_{h=1}^{h_{obs}} |F(h)|$, describing the quality of the experimental data.
§Difference R factor, $R_{diff} = \sum_{h=1}^{h_{obs}} |(F(h) - F^D(h))| / \sum_{h=1}^{h_{obs}} |F(h)|$, where $F(h)$ and $F^D(h)$ are the structure factors in the absence and presence of the peptide deuterium label. In all cases, $R_{diff} > R_{self}$.
¶Bragg spacing.

POPC bilayers containing 5 mol % $AcWL_5^H$ and $AcWL_5^{D23}$ and between POPC bilayers containing 5 mol % $AcWL_5^H$ and $AcWL_5^{D56}$. In both cases, no fit was achieved, implying that the deuterium label does not have a well-defined distribution.

In the previously published model of the membrane-bound $AcWL_5$ oligomer (see Fig. 11), the peptide resides in the hydrocarbon core of the bilayer (11,12). According to this model, the deuterated amino acids in $AcWL_5^{D23}$ and $AcWL_5^{D56}$ do not reside close to the edge of the unit cell. Therefore, a fit was attempted using the real space scaling procedure by assuming that the scattering length density profiles of POPC bilayers containing 5 mol % $AcWL_5^H$, $AcWL_5^{D23}$, and $AcWL_5^{D56}$ overlap at points z_1 and z_2 in the range 20–25 Å from the bilayer center (close to the edge of the unit cell). For all choices of z_1 and z_2, the fit yielded negative scaling factors, suggesting that the assumption that the deuterium distributions in $AcWL_5^{D12}$ and $AcWL_5^{D45}$ vanish at the edge of the unit cell is not correct.

Thus, scaling using the deuterated leucine label was not successful. Scaling was therefore performed using the D_2O label, despite the uncertainties in the measured hydration of the bilayer at 76% RH (see Materials and Methods). Whereas the absolute profiles in Fig. 6 depend on the hydration used in the calculation, their difference does not. The exact number of water molecules does not directly enter the calculation for the position and width of the water distribution; the only requirement for such calculation is the identical hydration of the two samples.

Measurements of water uptake were carried out gravimetrically; the measured value was 5 ± 1 waters/lipid. With this value, the bilayer profiles with 5 mol % $AcWL_5^H$, $AcWL_5^{D23}$, and $AcWL_5^{D56}$ were scaled independently. The absolute profiles are shown in Fig. 6 and then compared in Figs. 7 and 8. The values of the structure factors at 0% D_2O are presented in Table 1.

Fig. 7 *A* shows the scattering length density profiles for POPC bilayers containing 5 mol % $AcWL_5^H$ (*solid line*) and $AcWL_5^{D23}$ (*dashed line*). Fig. 8 *A* shows results for POPC bilayers containing 5% $AcWL_5^H$ (*solid line*) and $AcWL_5^{D56}$ (*dashed line*). Figs. 7 *B* and 8 *B* show difference profiles, reporting the distributions of the labeled leucines in $AcWL_5^{D23}$ and $AcWL_5^{D56}$. In sharp contrast to $AcWL_4$, no well-defined distribution of the label is observed in either case, suggesting a broad distribution of the deuterium label along the bilayer normal.

The Gaussian profiles describing the distribution of hydrating water can be obtained from the absolute structure profiles shown in Fig. 6. The center and width of the water distribution in the presence of $AcWL_5$ was calculated as 22.1 Å and 6.0 Å, respectively. The fitted water Gaussians are shown with the dashed lines in Fig. 9 *B*. The solid lines, which are in close agreement with the experimental profiles

TABLE 2 Difference structure factors describing the distributions of water at 76% RH

h*	$AcWL_4^H$	$AcWL_4^D$	$AcWL_5^H$	$AcWL_5^{D23}$	$AcWL_5^{D56}$
1	−3.78 ± 0.05	−4.17 ± 0.07	−3.36 ± 0.01	−3.32 ± 0.03	−3.31 ± 0.03
2	−2.42 ± 0.04	−2.65 ± 0.04	−1.84 ± 0.01	−1.76 ± 0.01	−1.72 ± 0.01
3	1.15 ± 0.04	1.17 ± 0.03	0.52 ± 0.01	0.44 ± 0.01	−0.42 ± 0.01
4	−0.39 ± 0.02	−0.43 ± 0.05	−0.03 ± 0.01	−0.08 ± 0.02	−0.03 ± 0.02
5			−0.06 ± 0.03	−0.11 ± 0.04	−0.08 ± 0.04

The values are obtained by subtracting the structure factors measured for 100% H_2O from the structure factors measured for 20% D_2O.
*Diffraction order.

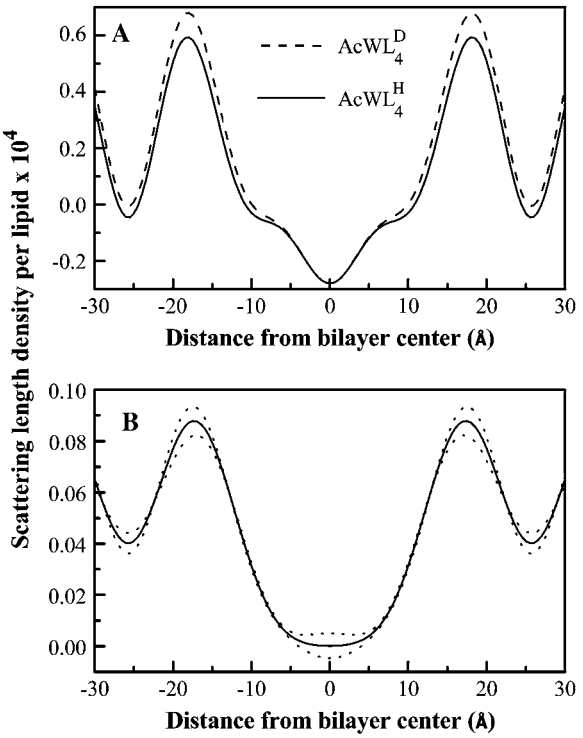

FIGURE 5 (*A*) Scattering length density profiles for POPC bilayers containing 5 mol % $AcWL_4^H$ (*solid line*) and $AcWL_4^D$ (*dashed line*). (*B*) The difference profile (*solid line*) corresponds to the transbilayer distribution of the deuterium label in $AcWL_4^D$. This profile reveals the location of the deuterated leucines in $AcWL_4^D$ as 17.1 ± 0.1 Å from the bilayer center. The dotted line depicts the uncertainty in the difference profile.

(*thick dotted lines*), are the envelopes of the two water Gaussians from apposing bilayers.

A question may arise whether lipids and peptides form separate phases, such that the peptide concentration in the multilayers giving rise to the Bragg peaks is very low (33), and thus the distribution of the deuterium label is hard to observe. To address this question, we inspected both the small- and the wide-angle signal using an area detector and x-ray diffraction. A homogeneous sample gives rise to a single set of Bragg peaks and a wide-angle diffuse peak that is very similar to the one observed for a pure fluid lipid bilayer. As discussed previously (33), a phase-separated sample shows either 1), two sets of Bragg peaks or 2), a single set of Bragg peaks identical to pure lipid samples and one or several sharp lines caused by protein aggregates appearing between the wide- and small-angle signals. We observed no indication for phase separation of $AcWL_5$ and POPC at 76% RH. Thus, peptides and lipids appear thoroughly mixed and form a single phase.

Furthermore, inspection of the crystallographic *R* factors presented in Table 1 shows that the contrast introduced by the deuterium label, as reported by R_{diff}, exceeds the random noise in the experimental structure factors, measured by R_{self}; i.e., $R_{diff} > R_{self}$. Therefore, the incorporation of the deuterated amino acids changes the structure factors and the scattering profiles, an indication that the peptide is present but the label is not well localized.

Structural insights from fluorescence studies

Additional structural information was sought by measuring tryptophan fluorescence in multilayer samples, to characterize the environment in which the $AcWL_4$ and $AcWL_5$ tryptophan residues reside. It is well documented that tryptophan fluorescence is sensitive to environmental factors such as polarity (34), and previous studies have shown that in liposomes, the tryptophan residues in both $AcWL_4$ and $AcWL_5$ are located in the interfacial region. Fig. 10 shows the fluorescence spectra of POPC oriented multilayers at 76% RH in the presence of 5 mol % $AcWL_5$ and $AcWL_4$. When tryptophan residues are buried deep within the bilayer hydrocarbon core, the emission maximum is ~320 nm (35). In the experimental spectra in Fig. 10, the peak maxima are ~340 nm, indicating that the tryptophan residues in both $AcWL_4$ and $AcWL_5$ are in the interface and not embedded in the hydrocarbon core of the bilayer. As discussed below, similar results were obtained for 100% humidity.

Refined molecular model of $AcWL_5$ in bilayers

Numerous spectroscopic and biophysical studies of $AcWL_5$, $AcWL_4$, and related peptides in bilayers (9–12,29,36) have

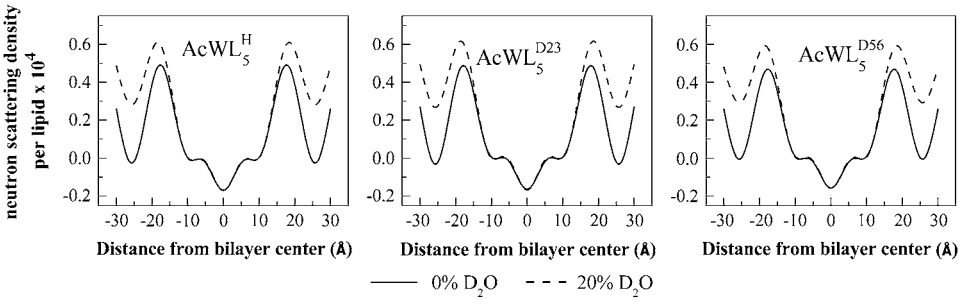

FIGURE 6 Absolute neutron-scattering length-density profiles of POPC bilayers with 5 mol % $AcWL_5$, $AcWL_5^{D23}$ and $AcWL_5^{D56}$. Profiles are shown for 0% D_2O (*solid lines*) and 20% D_2O (*dashed lines*). The differences between the profiles as a result of the isomorphous H_2O/D_2O replacement were used to scale the profiles assuming hydration of 5 waters per lipid. The measured value is 5 ± 1 waters per lipid, and the profile amplitudes depend on the particular value used (*not shown*). The differences between the dashed and the solid lines report the overlapping water distributions of apposing bilayers (see Fig. 9 for water distribution parameters).

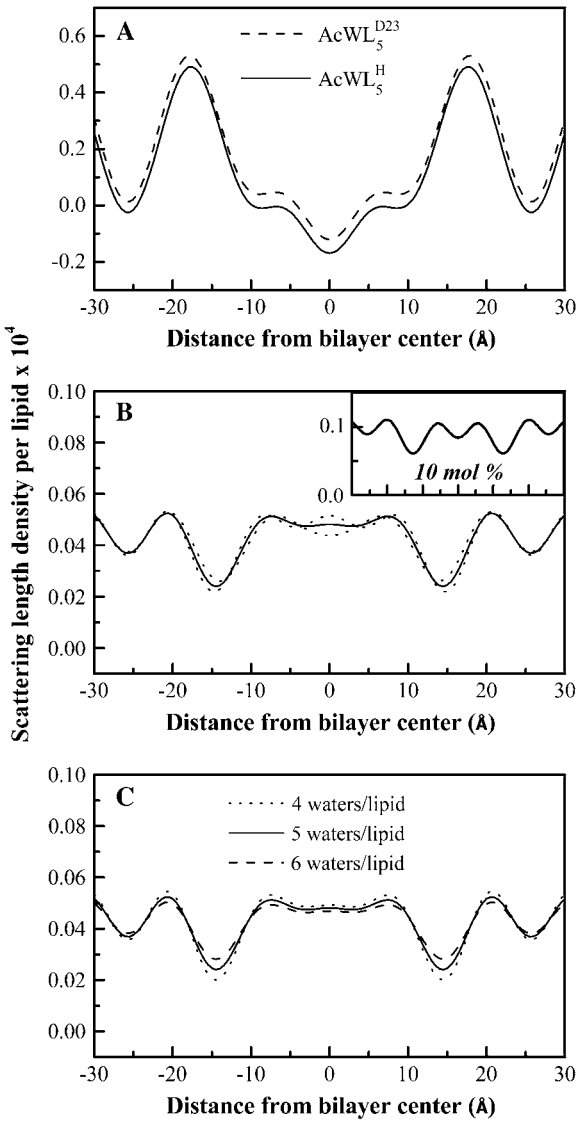

FIGURE 7 (*A*) Absolute scattering length density profiles for POPC bilayers containing 5 mol % $AcWL_5^{H}$ (*solid line*) and $AcWL_5^{D23}$ (*dashed line*). (*B*) The absolute difference profile, corresponding to the transbilayer distribution of the deuterium labels in $AcWL_5^{D23}$. The difference profile reports the location of the two N-terminal leucines in $AcWL_5$ with respect to the bilayer normal. No well-defined position can be determined. Results are the same for 10 mol % peptide (*inset*). The dotted lines represent the uncertainty in the difference profile caused by the experimental uncertainties in the measured structure factors. (*C*) The difference profiles calculated assuming 4, 5, and 6 waters (measured value is 5 ± 1 waters/lipid). Although the absolute profiles in Fig. 6 depend on the hydration used in the calculation, but their difference does not.

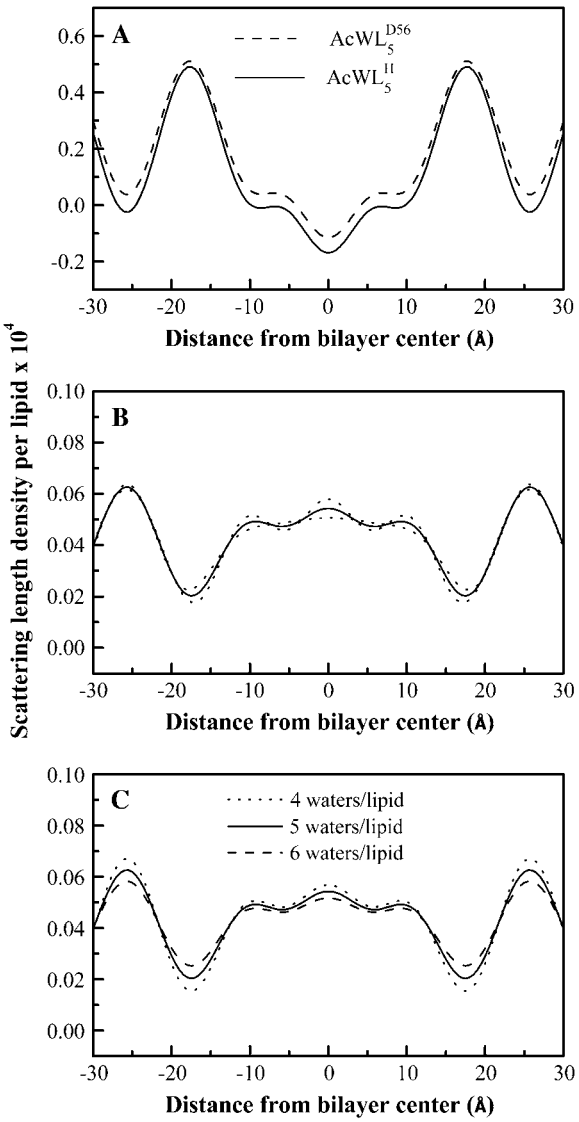

FIGURE 8 (*A*) Absolute scattering length density profiles for POPC bilayers containing 5 mol % $AcWL_5^{H}$ (*solid line*) and $AcWL_5^{D56}$ (*dotted line*). (*B*) The absolute difference profile (*solid line*) and experimental uncertainties (*dotted lines*), showing no defined location of the two C-terminal leucines in $AcWL_5$ within the bilayer. (*C*) The difference profile does not depend on the particular hydration level used in the scaling.

led to a model of a transmembrane, antiparallel $AcWL_5$ β-sheet, which we refine here using the information derived from neutron diffraction. The important past observations for $AcWL_5$ structure can be summarized as follows: 1), $AcWL_5$ forms highly ordered, antiparallel β-sheets in bilayers with an oligomer number around 10 (12); 2), cross-strand hydrogen bonds are perpendicular to the bilayer normal (12); 3), the tryptophan residues in the β-sheet are found in a homogeneous environment that is not deeply buried in the bilayer but instead is partially water exposed (11,12); 4), the middle leucine residue appears to be buried near the center of the bilayer's hydrocarbon core and interacts mainly with lipid, indicating that the β-sheets are single (isolated) sheets rather than stacked three-dimensional structures (11); 5), the terminal carboxyl group has a pK_a of ~5, indicating that it is exposed to water in the β-sheet (9); 6), $AcWL_5$ does not significantly disrupt the integrity of bilayers even at very high concentration (10 mol %) (12); 7), the end-to-end distance of $AcWL_5$ is ~18 Å, and the thickness of the

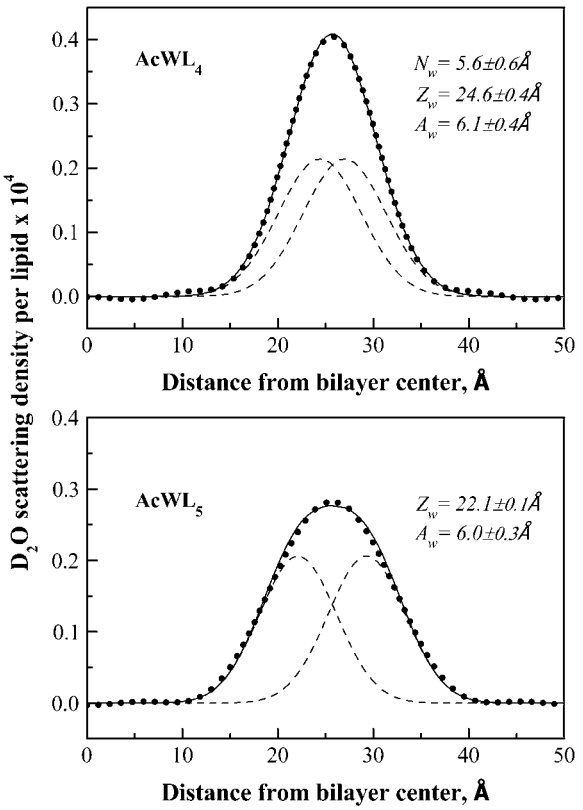

FIGURE 9 (*A*) Experimental (*thick dotted lines*) and fitted difference profiles describing the water distribution in bilayers with $AcWL_4$. The fitted water Gaussians, derived as described in Materials and Methods, are shown with the dashed lines. The solid lines are the envelopes of the two water Gaussians from apposing bilayers. (*B*) Fitted positions and widths of the water uptaken by POPC bilayers with $AcWL_5$. These parameters are calculated from the absolute profiles shown in Fig. 6 and do not depend on the hydration level used in the scaling. The fitted water Gaussians are shown with the dashed lines, and their envelope is shown with the solid line.

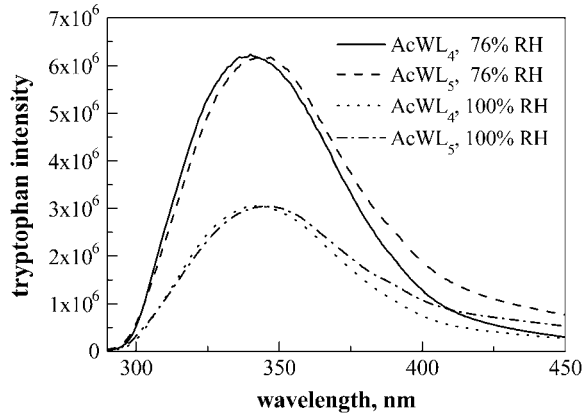

FIGURE 10 Tryptophan fluorescence emission spectra for POPC bilayers in the presence of 5 mol % $AcWL_4$ and $AcWL_5$. Data were acquired at 76% RH and 100% RH. In all cases, the peak maximum is ~340 nm, indicating that the tryptophan residues are located in the bilayer interface.

hydrocarbon core in these bilayers is ~30 Å; 8), a peptide with one additional leucine, $AcWL_6$, has the same secondary structure as $AcWL_5$ but is extremely stable and can not be unfolded under any conditions (9,12).

These previous observations led us to propose the model shown in Fig. 11 *A* in which the antiparallel $AcWL_5$ β-sheets are symmetric and centered in the hydrocarbon core of the bilayer to maximize the match in the hydrophobicity profiles of peptides and lipids. Because the hydrophobic thickness mismatch between peptide and bilayer is significant, we envisioned that bilayer thinning and disorder would have to occur around the β-sheets in the membrane. Using models like the one in Fig. 11 *A* as the basis for a hypothesis, we predicted that neutron diffraction experiments would detect distinct high-contrast peaks for the deuterated $AcWL_5$ molecules. Instead, what we observed was a continuum of deuterium across the bilayer, with no high-contrast peaks. This observation has led to a refined model of $AcWL_5$ β-sheets shown in Fig. 11, *B* and *C*, created as described in Materials and Methods. In this new model, most of the features of the previous model are retained; however, the β-strands are offset and staggered (not symmetrical) in their hydrogen bonding pattern, such that the depth of an individual residue in the bilayer is variable, and the width of the β-sheet is larger than the length of a single β-strand.

Further support for this model comes from comparing water distributions in POPC bilayers with $AcWL_4$ and $AcWL_5$, shown in Fig. 9. The comparison suggests that the water penetration into the bilayer in the presence of $AcWL_5$ is deeper than that in the presence of $AcWL_4$. The bilayers have the same Bragg's spacing, but the center of the water distribution is at 22.1 Å in the presence of $AcWL_5$ and at 24.6 Å in the presence of $AcWL_4$. This is consistent with the refined structural model: the water penetrates deeper into bilayers with $AcWL_5$ than with $AcWL_4$, by an additional 2.5 Å, covering an additional ~5 Å of the bilayer thickness.

Effects of hydration

The neutron diffraction experiments were carried out at low hydration, 76% RH. At high hydration, the lattice disorder in the samples is known to broaden the diffraction peaks until they cannot be resolved above the experimental noise (31). This can lead to inaccuracies in data interpretation and problems with absolute scaling. We have previously shown that the structure of the bilayer does not change much with hydration above 76% RH (21). A question remains, however, whether the disposition of the peptides changes on changes in hydration. As an example of a peptide that is highly sensitive to hydration changes, the pore-forming peptide alamethicin undergoes a transition from an interfacial to a TM orientation that can be easily followed using oriented CD (OCD) (37). We therefore compared OCD and fluorescence spectra of $AcWL_4$ and $AcWL_5$ at 76% RH and

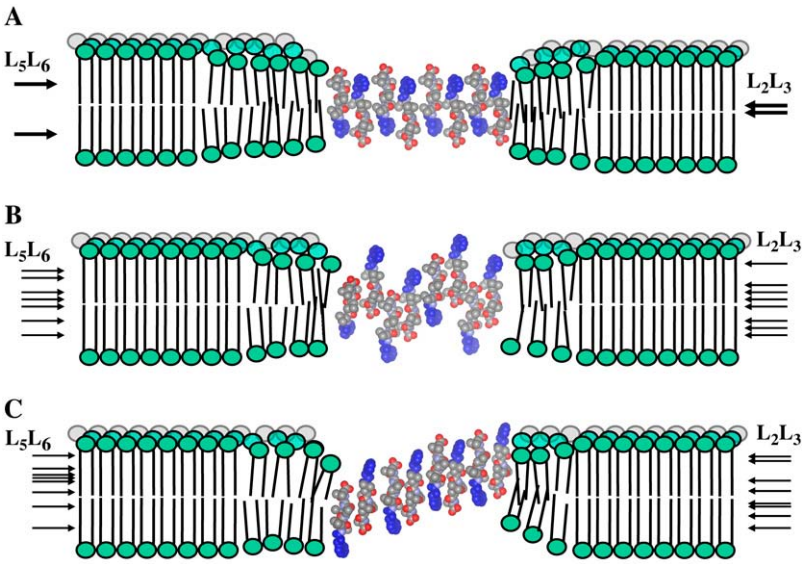

FIGURE 11 (*A*) Previous model and (*B* and *C*) revised models for $AcWL_5$ β-sheets in membranes. Previous models for the disposition of $AcWL_5$ β-sheets in membranes, such as the one shown in panel *A*, had been created by envisioning a structure that was driven by hydrophobic complementarity to reside in the middle of the bilayer. Such a structure would be symmetric, and some bilayer distortion at the peptide-water interface would be necessary to accommodate the relatively short peptide. Molecular modeling predicted that any symmetric structure would have given rise to distinct peaks in the neutron diffraction experiments for the transbilayer distribution of deuterons for either one or both of the deuterium-labeled peptides that we studied, L2L3 and L5L6. The centers of mass of the deuterons for model *A*, which are single Gaussian distributions in each monolayer, are shown at the left and right by black arrows. The revised models (*B* and *C*), which are consistent with the observed lack of distinct high-contrast peaks in neutron diffraction experiments, are characterized by β-strands that are staggered rather than symmetric. In panel *B*, we show a model with random stagger such that the effective width of the β-sheet may be close to the width of the hydrocarbon core. In panel *C*, a model with a unidirectional stagger is shown with some required bilayer distortion. The neutron diffraction data do not distinguish between these classes. For both staggered models, the positions of the deuteron centers of mass are different for each strand of the β-sheet. This is indicated by the arrows on the left and right, where each arrow shows the position of the labeled leucines in one peptide. Molecular modeling predicts that only staggered TM structures are consistent with the neutron diffraction experiments, whereas symmetrical structures always gave high-contrast peaks in the predicted transbilayer distributions of deuterium.

at 100% RH; the comparisons are shown in Figs. 2 and 10. Both the OCD and the fluorescence signals are nearly identical at 76% and 100% RH, demonstrating that the increase in hydration does not change the disposition of $AcWL_4$ and $AcWL_5$ in bilayers. Thus, structural information acquired at 76% should be relevant for higher hydration.

DISCUSSION

Experimental techniques for studies of membrane protein structure and utility of neutron diffraction

A detailed understanding of the principles of folding and structure of membrane proteins remains elusive because of the challenges in obtaining high-resolution structural data within the bilayer environment. Structural information on peptides and proteins in membranes is generally deduced using multiple independent techniques that separately provide only partial descriptions of structure. Spectroscopic techniques that can yield useful information in membranes include CD and OCD, Fourier transform infrared spectroscopy (FTIR), solid-state NMR, fluorescence, and EPR. CD measures overall secondary structure content, and OCD and solid-state NMR can determine orientation of helical segments in membranes (23,37–40). FTIR also reports on secondary structure content, and related methods such as polarized attenuated total reflectance FTIR can give information on the orientation of secondary structural elements in the bilayer (12,41,42). Fluorescence and EPR are used to estimate the depth of penetration of amino acids or probe moieties in the membrane and can sometimes reveal local secondary structure (43–47). Diffraction methods, using x rays or neutrons, have been used to obtain higher-resolution depth distributions of lipid or peptide moieties in the bilayer (16,20,48–51). Such diffraction methods have proven their utility in accurately showing the position and orientation of amphipathic helices in the bilayer interface (23,24) as well as the disposition of TM helices across the bilayer (16). Here we show that neutron diffraction results can be used to refine a structural model of a β-sheet oligomer in membranes that was based on CD, FTIR, and fluorescence (9–12). This work demonstrates that the combination of neutron diffraction with spectroscopic techniques can provide a more complete image of polypeptide structure in the membrane environment.

Structure of oligomeric $AcWL_5$ in lipid bilayers

The hexapeptide Acetyl-Trp-Leu_5 has been used as a model system for studying folding of proteins in membranes (9–12). It is soluble in aqueous buffers but binds to bilayers and assembles into β-sheets, which have been characterized by a variety of spectroscopic techniques. CD showed that $AcWL_5$ is a random coil in buffer and folds in membranes into oligomeric β-sheets by a pathway best described by a nucleation and growth mechanism (12). CD and calorimetry were used to show that the β-sheets unfold thermally and reversibly at ~65°C (11,12). The oligomer size from several modeling studies was estimated to be in the range of 3–10

or more peptides (9–12). FTIR was used to show that the β-sheets are antiparallel and that the cross-strand hydrogen bonds are parallel to the membrane surface, suggesting a TM orientation (12). The position of the N-terminal Trp residue in bilayers was probed by fluorescence spectroscopy. The emission maximum was at 340 nm, indicating an interfacial, water-exposed disposition. The shape and width of the emission spectra indicated that the Trp residues were present in a homogeneous chemical environment. This was supported by the observation that the Trp residue fluorescence is quenched by aqueous-phase quenchers. In this work (Fig. 10) we showed that the Trp fluorescence in oriented multilayers has an emission maximum of 342 nm at 76% RH and 344 nm at 100% RH, consistent with an interfacial, water-exposed disposition.

Similarly, pH studies indicated that the pK_a of the terminal carboxyl group is ~5, consistent with an interfacial location (9). Further evidence for a TM orientation was obtained in studies of homologous peptides of the form AcW-L-L-X-L-L, where X was any of the 20 amino acids (11). Only peptides with nonpolar X-residues (Ala, Leu, Ile, Val, Met, and Phe) supported β-sheet formation. The remainder of the peptides were monomeric, interfacially bound random coils that did not form β-sheets under any condition. Such strong disruption of β-sheet formation by polar moieties in the X-position is expected to occur only if the X-position of the β-sheet residues is in the hydrocarbon core of the membrane and not in the interface (36). At the same time, for those residues that supported sheet formation, the structure of the oligomer and the energetics of folding and unfolding were essentially identical, suggesting that the side chains in the TM β-sheets are interacting with lipid, whereas protein-protein interactions are mediated mainly by backbone hydrogen bonding. Taken together, these findings are consistent with the idea that the β-sheets formed by $AcWL_5$ in membranes are probably unstacked, antiparallel, TM sheets, ~10 peptides long.

These many experiments have constrained the potential structures for this peptide, and a model of a TM β-sheet has emerged (12). However, multiple structures are still possible, and the disposition of the peptides across the membrane is unknown. Here we used neutron diffraction of oligomeric $AcWL_5$ in bilayers to further constrain the structural model proposed on the basis of FTIR, CD, and fluorescence. In particular, we sought the depth of penetration of two different pairs of adjacent leucine residues of $AcWL_5$ within the bilayer thickness. Although the peptides were in the bilayer and had β-sheet structure, we found no well-defined peak or dip in the TM distribution, indicating heterogeneity in the TM location (Figs. 7 and 8). In other words, the labeled leucines were spread across the bilayer thickness. At the same time, residues of the monomeric homolog $AcWL_4$ exhibited a homogeneous, well-defined interfacial peak in the transbilayer distribution, with little or no peptide in the hydrocarbon core (Fig. 5). Taken together, the neutron diffraction, the previous spectroscopic results, and the molecular modeling discussed above give rise to a revised hypothetical structure for $AcWL_5$ in bilayers in which protein-protein interactions define a staggered TM β-sheet (Fig. 11). Thus, it appears that although the location of monomeric peptide segments in the bilayer is determined primarily by hydrophobic complementarity, protein-protein interactions in the $AcWL_5$ oligomer overshadow protein-lipid interactions and lead to variations in the depth of penetration of individual peptides in the bilayer.

Insights into membrane protein folding

The results presented here highlight a general principle in membrane protein folding. Although the position and orientation of isolated hydrophobic segments are determined by

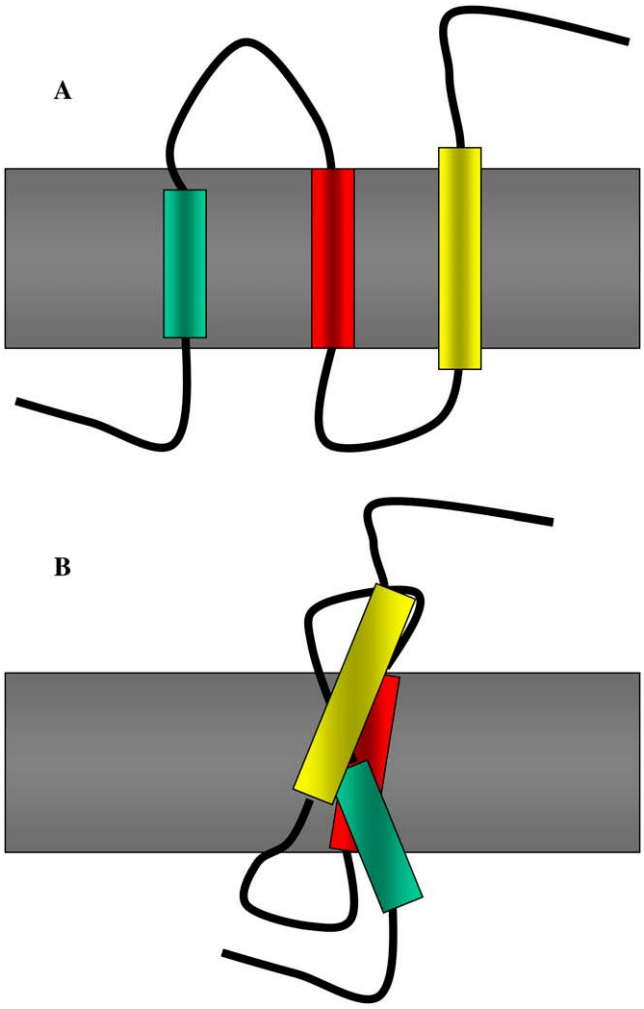

FIGURE 12 Augmented two-stage model of membrane protein folding. (*A*) Three isolated TM helices are shown embedded in a lipid bilayer. In the absence of protein-protein interactions, hydrophobic complementarity drives the helices to have their most hydrophobic segments aligned with the hydrocarbon core of the membrane. (*B*) A hypothetical folded membrane protein is shown in which specific protein-protein interactions contribute significantly to the disposition of the helices in the bilayer. This idea augments the popular two-stage model of membrane protein folding proposed by Popot and Engelman (52).

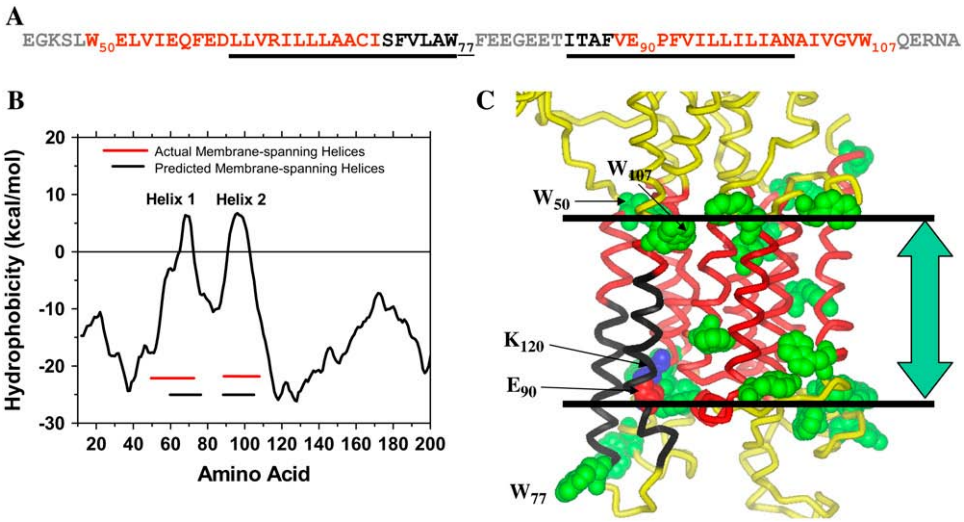

FIGURE 13 Interplay between hydrophobic complementarity and protein-protein interactions in a membrane protein structure. The first two helices of the calcium ATPase (53) are highlighted to show the principle. In panel *A*, the sequence containing the first two TM helices is shown. Actual TM helices are in red letters, and predicted helices are underlined in black. In panel *B*, we show the hydrophobicity profile that was used to predict the location of the two TM helices (4). There are two very sharp peaks in this 19-residue sliding window average that unambiguously define the center of a predicted TM helix. The black and red bars below the hydrophobicity profile represent the predicted and experimentally determined TM segments, respectively. In panel *C*, the structure of the protein is shown (53). The portion of the protein that is embedded in the 30 Å hydrocarbon core of the membrane is delineated by the two bands of aromatic residues, shown in green. The predicted boundaries of TM helices 1 and 2 are shown in black, and the actual TM helices are shown in red. The membrane-embedded portion of helix 1 has numerous polar and charged residues, and a highly hydrophobic stretch of 19 amino acids is only partially inserted into the membrane. This example demonstrates that the type of offset in hydrophobic complementarity that we deduced from the model β-sheet peptide structure is also observed in α-helical membrane proteins.

hydrophobic complementarity, the folded structure of the protein in the membrane is also influenced by protein-protein interactions. This principle is illustrated in Fig. 12. In panel *A* we show three TM helices, representing the most hydrophobic segments of 19 amino acids in the sequence. Hydrophobic complementarity determines the position of the isolated segments within the membrane. In panel *B*, the folded structure is shown in which protein-protein interactions have shifted the positions of the TM segments relative to the bilayer, such that hydrophobic matching is no longer the sole determinant of the TM disposition of the helices. We note that this principle augments the popular two-stage model of membrane protein folding, proposed by Popot and Engelman (52).

Current hydrophobicity scales are known to accurately predict the number of TM segments in α-helical membrane proteins (4). However, there are often discrepancies between the predicted and observed boundaries of the membrane-inserted segments (4). As a specific example, Fig. 13 shows the structure of the calcium ATPase transporter from rabbit sarcoplasmic reticulum (53), highlighting the first two TM helices. The bands of aromatic residues, in green, clearly delineate the 30-Å hydrocarbon core of the bilayer (54–56). Hydrophobicity-based prediction algorithms (4) correctly identify two helices in the region containing helices 1 and 2, but the actual depths of the predicted helices in the bilayer do not match the hydrocarbon core of the bilayer. Inspection of the sequence and structure in Fig. 13 reveals charged and polar residues in the hydrocarbon core of the bilayer, whereas the most hydrophobic segment of helix 1 extends well into a loop on the luminal surface of the protein. Van der Waals knob-into-hole packing interactions between hydrophobic amino acid chains on the luminal side of the two helices and hydrogen bonding interactions between membrane-embedded polar residues, such as the interaction between Glutamate-90 on helix 2 and Lysine-120 on helix 3 (Fig. 13), probably stabilize the exact disposition of these helices in the bilayer. This example demonstrates that the type of offset in hydrophobic complementarity, driven by protein-protein interactions, that we deduced from the model β-sheet peptide structure is also observed in α-helical membrane proteins.

We thank Drs. M. Mihailescu and D. Worcester for their help with neutron data collection and processing and for useful discussions.

This work was supported by National Institutes of Health grants GM068619 (K.H.) and GM060000 (W.C.W). We acknowledge the support of the National Institute of Standards and Technology, U.S. Department of Commerce, and the Cold Neutrons for Biology and Technology program funded by the National Institutes of Health under grant RR14812, and the Regents of the University of California for providing the neutron research facilities used in this work.

REFERENCES

1. Wiener, M. C., and S. H. White. 1992. Structure of a fluid dioleoylphosphatidylcholine bilayer determined by joint refinement of x-ray and neutron diffraction data. III. Complete structure. *Biophys. J.* 61:434–447.
2. White, S. H., A. S. Ladokhin, S. Jayasinghe, and K. Hristova. 2001. How membranes shape protein structure. *J. Biol. Chem.* 276:32395–32398.
3. White, S. H., and W. C. Wimley. 1999. Membrane protein folding and stability: physical principles. *Annu. Rev. Biophys. Biomol. Struct.* 28:319–365.

4. Jayasinghe, S., K. Hristova, and S. H. White. 2001. Energetics, stability, and prediction of transmembrane helices. *J. Mol. Biol.* 312:927–934.
5. Hildebrand, P. W., S. Lorenzen, A. Goede, and R. Preissner. 2006. Analysis and prediction of helix-helix interactions in membrane channels and transporters. *Proteins.* 64:253–262.
6. Eyre, T. A., L. Partridge, and J. M. Thornton. 2004. Computational analysis of alpha-helical membrane protein structure: implications for the prediction of 3D structural models. *Protein Eng. Des. Sel.* 17:613–624.
7. Liu, W., M. Eilers, A. B. Patel, and S. O. Smith. 2004. Helix packing moments reveal diversity and conservation in membrane protein structure. *J. Mol. Biol.* 337:713–729.
8. Schneider, D. 2004. Rendezvous in a membrane: close packing, hydrogen bonding, and the formation of transmembrane helix oligomers. *FEBS Lett.* 577:5–8.
9. Wimley, W. C., and S. H. White. 2004. Reversible unfolding of beta-sheets in membranes: a calorimetric study. *J. Mol. Biol.* 342:703–711.
10. Paul, C., J. Wang, W. C. Wimley, R. M. Hochstrasser, and P. H. Axelsen. 2004. Vibrational coupling, isotopic editing, and beta-sheet structure in a membrane-bound polypeptide. *J. Am. Chem. Soc.* 126: 5843–5850.
11. Bishop, C. M., W. F. Walkenhorst, and W. C. Wimley. 2001. Folding of β-sheet membrane proteins: Specificity and promiscuity in peptide model systems. *J. Mol. Biol.* 309:975–988.
12. Wimley, W. C., K. Hristova, A. S. Ladokhin, L. Silvestro, P. H. Axelsen, and S. H. White. 1998. Folding of β-sheet membrane proteins: A hydrophobic hexapeptide model. *J. Mol. Biol.* 277:1091–1110.
13. Grant, G. A. 1992. Synthetic Peptides: A User's Guide. W. H. Freeman and Company, New York.
14. Atherton, E., and R. C. Sheppard. 1989. Solid Phase Peptide Synthesis. IRL Press, Oxford, UK.
15. Iwamoto, T., M. You, E. Li, J. Spangler, J. M. Tomich, and K. Hristova. 2005. Synthesis and initial characterization of FGFR3 transmembrane domain: consequences of sequence modifications. *Biochim. Biophys. Acta.* 1668:240–247.
16. Han, X., M. Mihailescu, and K. Hristova. 2006. Neutron diffraction studies of fluid bilayers with transmembrane proteins: structural consequences of the achondroplasia mutation. *Biophys. J.* 91:3736–3747.
17. Jacobs, R. E., and S. H. White. 1987. Lipid bilayer perturbations induced by simple hydrophobic peptides. *Biochemistry.* 26:6127–6134.
18. Wiener, M. C., and S. H. White. 1991. Fluid bilayer structure determination by the combined use of x-ray and neutron diffraction. I. Fluid bilayer models and the limits of resolution. *Biophys. J.* 59:162–173.
19. Wiener, M. C., and S. H. White. 1991. Fluid bilayer structure determination by the combined use of x-ray and neutron diffraction. II. ''Composition-space'' refinement method. *Biophys. J.* 59:174–185.
20. Wiener, M. C., and S. H. White. 1991. Transbilayer distribution of bromine in fluid bilayers containing a specifically brominated analog of dioleoylphosphatidylcholine. *Biochemistry.* 30:6997–7008.
21. Hristova, K., and S. H. White. 1998. Determination of the hydrocarbon core structure of fluid dioleoylphosphocholine (DOPC) bilayers by x-ray diffraction using specific bromination of the double-bonds: Effect of hydration. *Biophys. J.* 74:2419–2433.
22. Wiener, M. C., G. I. King, and S. H. White. 1991. Structure of a fluid dioleoylphosphatidylcholine bilayer determined by joint refinement of x-ray and neutron diffraction data. I. Scaling of neutron data and the distribution of double-bonds and water. *Biophys. J.* 60:568–576.
23. Hristova, K., W. C. Wimley, V. K. Mishra, G. M. Anantharamiah, J. P. Segrest, and S. H. White. 1999. An amphipathic α-helix at a membrane interface: a structural study using a novel x-ray diffraction method. *J. Mol. Biol.* 290:99–117.
24. Hristova, K., C. E. Dempsey, and S. H. White. 2001. Structure, location, and lipid perturbations of melittin at the membrane interface. *Biophys. J.* 80:801–811.
25. Merzlyakov, M., E. Li, R. Casas, and K. Hristova. 2006. Spectral Forster resonance energy transfer detection of protein interactions in surface-supported bilayers. *Langmuir.* 22:6986–6992.
26. Li, E., M. You, and K. Hristova. 2006. FGFR3 dimer stabilization due to a single amino acid pathogenic mutation. *J. Mol. Biol.* 356:600–612.
27. Crowe, J. H., B. J. Spargo, and L. M. Crowe. 1987. Preservation of dry liposomes does not require retention of residual water. *Proc. Natl. Acad. Sci. USA.* 84:1537–1540.
28. Berman, H. M., J. Westbrook, Z. Feng, G. Gilliland, T. N. Bhat, H. Weissig, I. N. Shindyalov, and P. E. Bourne. 2000. The Protein Data Bank. *Nucleic Acids Res.* 28:235–242.
29. Wimley, W. C., and S. H. White. 1996. Experimentally determined hydrophobicity scale for proteins at membrane interfaces. *Nat. Struct. Biol.* 3:842–848.
30. Johnson, W. C. 1988. Secondary structure of proteins through circular dichroism spectroscopy. *Annu. Rev. Biophys. Biophys. Chem.* 17: 145–166.
31. Zhang, R.-T., S. Tristram-Nagle, W.-J. Sun, R. L. Headrick, T. C. Irving, R. M. Suter, and J. F. Nagle. 1996. Small-angle x-ray scattering from lipid bilayers is well described by modified Caillé theory but not by paracrystalline theory. *Biophys. J.* 70:349–357.
32. Chakrabartty, A., T. Kortemme, S. Padmanabhan, and R. L. Baldwin. 1993. Aromatic side-chain contribution to the far-ultraviolet circular dichroism of helical peptides and its effect on measurement of helix propensities. *Biochemistry.* 32:5560–5565.
33. You, M., E. Li, W. C. Wimley, and K. Hristova. 2005. Forster resonance energy transfer in liposomes: measurements of transmembrane helix dimerization in the native bilayer environment. *Anal. Biochem.* 340:154–164.
34. Lakowicz, J. R. 1983. Principles of Fluorescence Spectroscopy. Plenum Press, New York.
35. Ladokhin, A. S., S. Jayasinghe, and S. H. White. 2000. How to measure and analyze tryptophan fluorescence in membranes properly, and why bother? *Anal. Biochem.* 285:235–245.
36. Wimley, W. C., T. P. Creamer, and S. H. White. 1996. Solvation energies of amino acid sidechains and backbone in a family of host-guest pentapeptides. *Biochemistry.* 35:5109–5124.
37. Wu, Y., H. W. Huang, and G. A. Olah. 1990. Method of oriented circular dichroism. *Biophys. J.* 57:797–806.
38. Wimley, W. C., and S. H. White. 2000. Designing transmembrane α-helices that insert spontaneously. *Biochemistry.* 39:4432–4442.
39. Opella, S. J., J. Gesell, and B. Bechinger. 1993. NMR spectroscopy of amphipathic helical peptides in membrane environments. *In* The Amphipathic Helix. R. M. Epand, editor. CRC Press, Boca Raton, FL. 87–106.
40. Bechinger, B. 2001. Membrane insertion and orientation of polyalanine peptides: a (15)N solid-state NMR spectroscopy investigation. *Biophys. J.* 81:2251–2256.
41. Citra, M. J., and P. H. Axelsen. 1996. Determination of molecular order in supported lipid membranes by internal reflection Fourier transform infrared spectroscopy. *Biophys. J.* 71:1796–1805.
42. Rothschild, K. J. 1992. FTIR difference spectroscopy of bacteriorhodopsin: Toward a molecular model. *J. Bioenerg. Biomembr.* 24:147–167.
43. Ramachandran, R., A. P. Heuck, R. K. Tweten, and A. E. Johnson. 2002. Structural insights into the membrane-anchoring mechanism of a cholesterol-dependent cytolysin. *Nat. Struct. Biol.* 9:823–827.
44. Altenbach, C., J. Klein-Seetharaman, J. Hwa, H. G. Khorana, and W. L. Hubbell. 1999. Structural features and light-dependent changes in the sequence 59–75 connecting helices I and II in rhodopsin: a site-directed spin-labeling study. *Biochemistry.* 38:7945–7949.
45. Voss, J., W. L. Hubbell, and H. R. Kaback. 1998. Helix packing in the lactose permease determined by metal-nitroxide interaction. *Biochemistry.* 37:211–216.
46. Wang, Q. D., J. Voss, W. L. Hubbell, and H. R. Kaback. 1998. Proximity of helices VIII (Ala273) and IX (Met299) in the lactose permease of *Escherichia coli*. *Biochemistry.* 37:4910–4915.
47. Posokhov, Y. O., and A. S. Ladokhin. 2006. Lifetime fluorescence method for determining membrane topology of proteins. *Anal. Biochem.* 348:87–93.

48. Bradshaw, J. P., M. J. Darkes, T. A. Harroun, J. Katsaras, and R. M. Epand. 2000. Oblique membrane insertion of viral fusion peptide probed by neutron diffraction. *Biochemistry.* 39:6581–6585.

49. Dante, S., T. Hauss, and N. A. Dencher. 2002. Beta-amyloid 25 to 35 is intercalated in anionic and zwitterionic lipid membranes to different extents. *Biophys. J.* 83:2610–2616.

50. Hauss, T., S. Dante, T. H. Haines, and N. A. Dencher. 2005. Localization of coenzyme Q10 in the center of a deuterated lipid membrane by neutron diffraction. *Biochim. Biophys. Acta.* 1710:57–62.

51. Gawrisch, K., H. C. Gaede, M. Mihailescu, and S. H. White. 2007. Hydration of POPC bilayers studied by (1)H-PFG-MAS-NOESY and neutron diffraction. *Eur. Biophys. J.* 36:281–291.

52. Popot, J.-L., and D. M. Engelman. 1990. Membrane protein folding and oligomerization—the 2-stage model. *Biochemistry.* 29:4031–4037.

53. Toyoshima, C., M. Nakasako, H. Nomura, and H. Ogawa. 2000. Crystal structure of the calcium pump of sarcoplasmic reticulum at 2.6 A resolution. *Nature.* 405:647–655.

54. Wimley, W. C. 2003. The versatile beta-barrel membrane protein. *Curr. Opin. Struct. Biol.* 13:404–411.

55. Wimley, W. C. 2002. Toward genomic identification of beta-barrel membrane proteins: composition and architecture of known structures. *Protein Sci.* 11:301–312.

56. Schiffer, M., C. H. Chang, and F. J. Stevens. 1992. The functions of tryptophan residues in membrane proteins. *Protein Eng.* 5:213–214.